



In situ ex-solution of CoFeRu solid solution nanoparticles from non-stoichiometric $(\text{La}_{0.8}\text{Sr}_{0.2})_{0.9}\text{Co}_{0.1}\text{Fe}_{0.8}\text{Ru}_{0.1}\text{O}_{3-\delta}$ perovskite for hydrogen gas sensor

Bharat Sharma^{a,*}, Mukesh Kumar^b, Ashutosh Sharma^{c,*}

^a Institute of Microstructure Technology, Karlsruhe Institute of Technology, Hermann-Von-Helmholtz-Platz 1, Eggenstein-Leopoldshafen 76344, Germany

^b Department of Physics, Faculty of Applied and Basic Sciences, SGT University, Gurugram 122505, India

^c Amity Institute of Applied Sciences, Amity University, Ranchi, Jharkhand 834002, India

ARTICLE INFO

Keywords:

Ex-solution
Gas sensor
Nanoparticles
Perovskite
Reduction
Ruthenium
Hydrogen

ABSTRACT

Ex-solution process is a novel technology to grow uniformly distributed highly catalytic nanoparticles (NPs) on the surface of parent metal oxide solid support and has been recently applied to diverse engineering applications. Here, we study the effect of CoFeRu NPs which are ex-solved on the surface of Ru-doped $\text{La}_{0.8}\text{Sr}_{0.2}\text{Co}_{0.1}\text{Fe}_{0.9}\text{O}_{3-\delta}$ (LSCF) perovskite at reduction temperature 350–550 °C. The shape and size of decorated CoFeRu NPs on the surface of the (LSCFRu, $\text{La}_{0.8}\text{Sr}_{0.2}\text{Co}_{0.1}\text{Fe}_{0.8}\text{Ru}_{0.1}\text{O}_{3-\delta}$) sensing layer was studied for controlled hydrogen gas sensing. The results show that the ex-solved LSCFRu sensor leads to an enhanced gas response, long-term stability, and a smaller limit of detection (LOD=0.05 ppm) against H_2 gas exposure at 450 °C. The hydrogen gas sensing properties of ex-solved LSCFRu, $\text{La}_{0.8}\text{Sr}_{0.2}\text{Co}_{0.1}\text{Fe}_{0.8}\text{Ru}_{0.1}\text{O}_{3-\delta}$, is ($R_a/R_g = 55$) after reduction at 450 °C was enhanced to 20-folds compared to un-doped LSCF with a detection limit of 0.05 ppm. The high gas response is ascribed to the catalytic effect of uniformly embedded CoFeRu NPs ex-solved via p-to-n type transition of the LSCFRu parent oxide after reduction. The concept demonstrated here may serve in the development of potential ex-solved perovskite sensors for advanced and reliable hydrogen gas sensing.

1. Introduction

The advancements in materials research have led to a significant increase in the number of new gas sensing materials available, providing a broader basis for a wider choice and the development of high-performance chemiresistive gas sensors [1,2]. Hydrogen (H_2), being the lightest element in the periodic table, spreads speedily in our surroundings and requires close monitoring during its handling, storage, and transportation [3,4]. Moreover, H_2 is the supporting career for various petroleum industries in the production of CH_3OH and NH_3 . Therefore, there is a significant challenge associated with the storage and handling of H_2 gas when present in an explosive range (> 4% concentration) [5].

In order to meet these requirements, gas sensors must exhibit significantly improved gas response, selectivity, and stability to surpass the desired standards. For decades, metal oxide semiconductors (MOX) have been used in high-temperature applications, displaying reasonably high response and recovery, and precise limit of detection at sub-ppm

levels [6,7]. However, high temperatures (> 500 °C) can cause instability in gas response due to the thinning of charge depletion layer at the grain boundaries. There have been efforts to replace high-temperature oxides in order to achieve long-term stability in gas sensing in extreme conditions [8,9].

In contrast to MOX sensors, perovskite-based chemiresistive gas sensors have attracted sensor research community owing to faster adsorption kinetics and high thermal stability against harsh conditions [10–13]. The sensing layer plays an important role in chemiresistive gas sensors because the sensing performance is the function of key 3S parameters (sensitivity, selectivity, and stability) [14,15]. The uniform distribution of the highly catalytic NPs on the parent oxide support is important for improving adsorption-desorption kinetics in gas sensing [16–18].

Recent studies on perovskites-based chemiresistors demonstrate the in-situ growth of NPs in the gas sensor field due to their attractive electro-catalytic properties when reduced at high temperatures [19–21]. This class of ABO_3 oxides with big A-site cations and small B-site anions

* Corresponding authors.

E-mail addresses: bharat.sharma@kit.edu (B. Sharma), stannum.ashu@gmail.com (A. Sharma).

<https://doi.org/10.1016/j.snb.2024.136529>

Received 12 January 2024; Received in revised form 8 August 2024; Accepted 23 August 2024

Available online 3 September 2024

0925-4005/© 2024 The Authors. Published by Elsevier B.V. This is an open access article under the CC BY license (<http://creativecommons.org/licenses/by/4.0/>).

can be tuned by substituting for A and B sites with various transition element dopants. This type of doping of perovskite crystals renders the growth of ex-solved NPs selectively on the surface when host oxide is partially reduced at elevated temperatures [22]. Due to this freedom of material ex-solution, perovskites are now being employed in a variety of areas such as catalysis, fuel cells, and solid electrolytes, including gas sensing [23–28]. The ex-solved NPs exhibit enhance high-temperature and chemical stability to agglomeration and improve gas response compared to ex-situ NPs decorated sensors [29,30]. Due to these advantages of perovskite oxides and their wide range of compositions, ex-solution is beneficial for promoting their use in chemiresistive gas sensing applications.

Studies have reported the growth of in-situ NPs from the parent oxide host utilized for several gas sensing applications, such as PbTiO₃ used to detect ethanol and La_{1-x}Ca_xFeO₃ utilized for CO sensing [31,32]. Dai et al. reported that Ag NPs decorated AgNbO₃ sensor enabled superior sensitivity, selectivity, and stability towards NH₃ gas sensing [21]. Jang et al. developed Ir-Ex-solved WO₃ NPs for H₂S sensing and reported that a fine distribution of Ir-ex-solved NPs to the host oxide improved the H₂S gas response and selectivity with long-time stability [33]. In parent perovskite host, the alkaline earth elements occupy A-site (Ca, La, Pr, Ce, Ba, Sr, etc) while transition elements (Co, Fe, Mn, Ni, etc.) occupy B-site. Various dopants (Co, Ni, Fe, Mn, Mo, etc.) have been used to dope A or B-site to optimize the catalytic activity of oxide [34,35]. Recently, Kim et al. demonstrated a novel approach to develop ethanol gas sensors based on La_{0.43}Ca_{0.37}Co_{0.06}Ti_{0.94}O_{3-d} perovskite host with Co-ex-solved NPs. The Co-ex-solved NPs triggered the gas response and selective detection of ethanol remarkably [36]. In most of these ex-solution reports, monometallic ex-solution of NPs has been obtained which may trigger the tendency to aggregate and affect the stability of the sensor. A few notable bimetallic catalysts (Co-Mo, Ru-Fe, and Ni-Ru) have been used to improve the stability and activity of host oxide [37–39]. The use of multi-metal alloy NPs could be beneficial. However, the ex-solution of a parent host with more than two reducible dopants has rarely been employed. The ex-solution pattern of multi-dopants in host oxide should be studied as it may open up the possibility to tailor the composition space of host oxide. Additionally, multi-metallic alloy NPs grown on the parent oxide support will facilitate the adsorption-desorption kinetics and thus it could be a better approach for designing chemiresistive gas sensing.

In this study, a facile ex-solution process was used to engineer CoFeRu NPs-decorated perovskite oxide for chemiresistive H₂ sensing. The non-stoichiometric perovskite-type (La_{0.8}Sr_{0.2})_{0.9}Co_{0.1}Fe_{0.8}Ru_{0.1}O_{3-δ} (LSCFRu) was synthesized by solid-state alloying route and sintering methods. This approach resulted in improved gas response and low LOD of the H₂ sensor, along with enhanced selectivity and long-term durability. The parent oxide (LSCFRu) was produced and reduced at elevated temperatures to ex-solve the CoFeRu NPs on its surface. This method of ex-solving solid solution NPs for parent oxide has the potential to achieve high gas response, high selectivity, and long-term stability for sensing applications, making it a promising option for next-generation smart gas sensors.

2. Experimental

2.1. Preparation of parent LSCF sensing powder

(La_{0.8}Sr_{0.2})_{0.9}Co_{0.1}Fe_{0.9}O_{3-δ} (LSCF) and (La_{0.8}Sr_{0.2})_{0.9}Co_{0.1}Fe_{0.8}Ru_{0.1}O_{3-δ} (LSCFRu) powders were prepared by the solid-state alloying route. Stoichiometric amounts of La₂O₃, Co₂O₃, Fe₂O₃, SrCO₃ and RuO₂ powders (99.7 %, Sigma Aldrich, USA) were milled for 2 h in a planetary ball mill using ethanol as a process control agent. The Ar atmosphere was used to avoid oxidation of the powder mixture. The milled mixture was dried overnight at 80 °C and isostatic pressing in a green pellet at 1000 °C for 3 h. After the resultant gray pellet was calcined at 1400 °C for 5 h to obtain single phase perovskite host. The

calcined powder was ground in a mortar pestle (4 h) again for further electrode preparation and characterization studies.

2.2. Decoration of the LSCF to CoFeRu NPs

The as-fabricated perovskites were placed in a quartz vessel and reduced at different annealing temperatures (T = 350–450 °C) for 4 h in a mixture of 15 % H₂+Ar mixture. After the ex-solution of LSCFRu, the samples were annealed at various temperatures in Ar atmosphere for sensor preparation.

2.3. Sensor preparation

The sensitive layer was prepared by drop-casting LSCFRu on a Si wafer (12 × 12 mm²) with a Pt electrode. The drop-casting solution was prepared by mixing LSCFRu powder with deionized water followed by ultrasonication for 3 h. The as-prepared sensor electrodes were annealed at 650 °C for 3 h to eliminate the residual impurities followed by cooling down to room temperature (RT) before being inserted into a quartz vessel coupled with the furnace.

2.4. Gas sensing

The gas response was determined using a four-way valve to alternate between air and a target gas at a flow rate of 200 cm³/min. A personal computer and an electrometer (6487 Keithley Ammeter, Tecktronix, USA) were used to measure the DC two-probe current resistance. Gas responses to 5 ppm of H₂, NO, NO₂, CO, NH₃, HCHO were measured in the temperature range of 350–550 °C. The gas response was calculated as $S = R_a/R_g$ and R_g/R_a , where R_a and R_g represented the sensor resistance in air and target gas, respectively. The dynamic resistance response curves of different sensors at different H₂ concentrations (0.05–5 ppm) were measured. The response (t_{res}) and recovery (t_{rec}) times are expressed as:

$$t_{(res/rec)} = t(90\% \text{ of total}) - t(\text{initial}). \quad (2)$$

Here, $t_{(res)}$ denotes the response time when resistance grows to 90 % of the current, and $t_{(rec)}$ is the time consumed during the 90 % recovery of the current in the air.

2.5. Characterization details

The structural characterization of the samples was done by X-ray diffraction (XRD, Bruker D8 Advance, Germany) studies. The composition and microstructure of the samples were examined by field emission scanning electron microscopy (FE-SEM, Hitachi 4800S, Japan), energy dispersive X-ray spectroscopy (EDS, Oxford, INCA, UK), and transmission electron microscopy (TEM, Phillips, G20 twin, USA). The X-ray photoelectron spectroscopy (XPS) of the samples was analyzed using a Thermo ESCALAB 250 with Al K α radiation accelerated at 1486.6 eV and was calibrated with a C 1s peak at 284.6 ± 0.1 eV.

3. Results and discussion

The experimental procedure is illustrated in Fig. 1a. The impact of reduction temperature (350–550 °C) on the crystalline structure of LSCFRu and the size distribution of ex-solved CoFeRu NPs is shown in a sequence. The samples are designated as base host oxide (LSCF), doped host oxides (LSCFRu, Ex0) after reduction at 350, 450 and 550 °C by Ex_350, Ex_450, and Ex_550. While La, Sr, Co, Fe, and Ru in LSCFRu have oxidation states of +3, +2, +3, (+3 and +4), and +4, respectively. Here, Co, Fe, and Ru form a solid solution in this oxide because of their similar crystal structures, atomic sizes, and valence states. Moreover, they have a similar ionic radius, with Co³⁺ (0.645 Å), Fe²⁺ (0.645 Å), and Ru⁴⁺ (0.685 Å). The ionic radius of La³⁺ is approximately 1.06 Å and the ionic radius of Sr²⁺ is approximately 1.18 Å. According to Goldschmidt's rules, the formation of a solid solution is favored if the

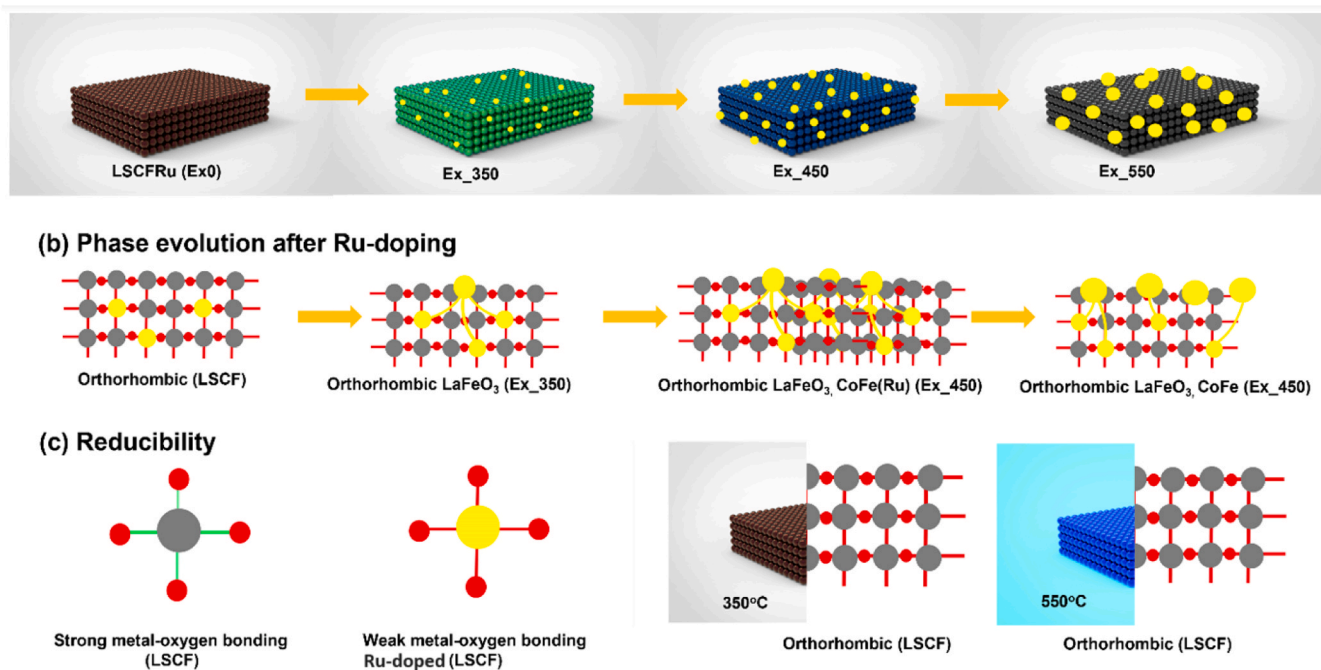


Fig. 1. (a) Schematics for the ex-solution of CoFeRu NPs-loaded LSCF sensors at different reductive conditions, (b) phase evolution after Ru-doping, and (c) reducibility of host oxide before and after doping.

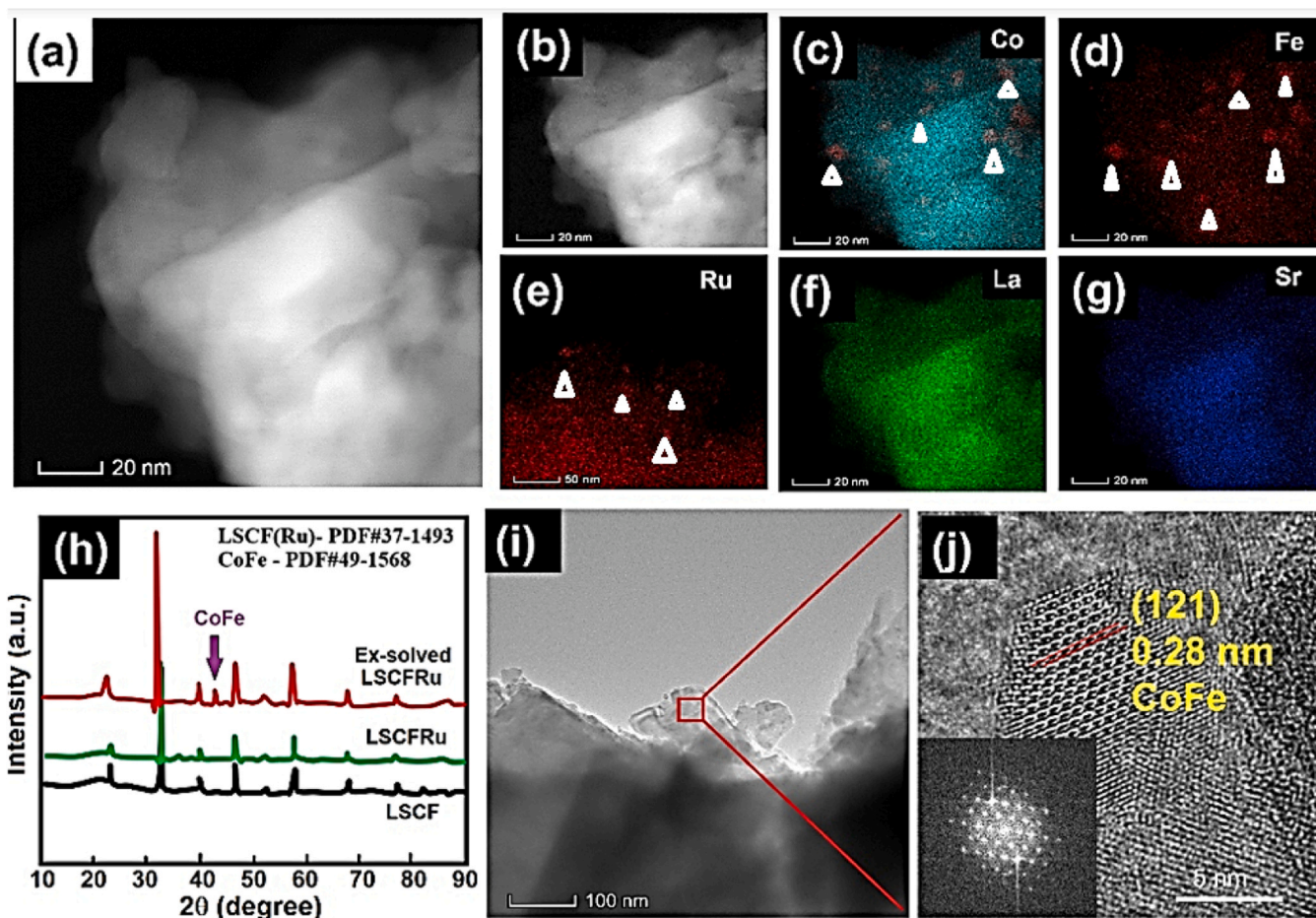


Fig. 2. (a) TEM image of LSCFRu electrode. (b-g) EDS mapping analysis of LSCFRu. (h) XRD patterns of different ex-solved LSCFRu, (i-j) High-resolution TEM images of LSCFRu annealed in 15% H₂/Ar mixture at 450 °C with corresponding FFT pattern.

difference in ionic radii $< 15\%$ [40]. The phase structure remains unchanged after the Ru doping of host oxide and the subsequent ex-solution process. The orthorhombic phase (LaFeO_3) was maintained after ex-solution (Fig. 1b-c). The weak bonding of Co-O, and Fe-O thus causes it to segregate over the host oxide surface. This makes it possible for host oxide to substitute for each other in the crystal lattice, forming a CoFeRu solid solution. Therefore, substituting Ru improves reducibility of LSCF (Fig. 1c) and facilitates phase evolution to more stable structures, improves catalytic activity and stability.

Our observations demonstrated that these phenomena greatly enhance the evolution of CoFeRu solid solution NPs, resulting in the uniformly ex-solved NPs at a low temperature $\approx 350^\circ\text{C}$. This is the extremely low temperature used for generating ex-solution NPs, even when highly reducible elements such as Ru, Pd, Ag, Au, Pt, and Ir are considered (Supplementary Tables S1). Additionally, our investigation is the first successful ex-solution utilizing solid solution-based ex-solved NPs for gas sensing. The LSCF sheets decorated with CoFeRu NPs had a high specific area of $16.74\text{ m}^2/\text{g}$, as measured in supporting Figure S1.

The TEM images of as-prepared porous LSCFRu electrodes are shown in Fig. 2a. The uniform dispersion of the elements Ru, Co, Fe, La, Sr, and O was confirmed through EDS analysis (Fig. 2b-g). The contour of Ru differs slightly from other EDS maps (Fig. 2b, e) because of the increased density of CoFe alloys in the presence of Ru dopants. It has been already reported that CoFe alloys can be ex-solved from $\text{La}_{0.4}\text{Sr}_{0.6}\text{Co}_{0.2}\text{Fe}_{0.8}\text{O}_{3-\delta}$ under reducing surroundings [35,36]. An additional doping of Ru in B-site could influence the segregation energy of Co and Fe ions in the site therefore promote or suppress the ex-solution of the CoFe alloys in the presence of dopants [41]. Additionally, the XRD patterns of the

Ru-doped LSCF revealed an orthorhombic LaFeO_3 phase (PDF#37-1493) without any other phase (Fig. 2h). With loading Ru in the first reduction step, weak phase transformation and RuFe alloy phase appears and then loaded structure evolved back to the original perovskite after reoxidation and ex-solved process. Such observations have been noticed during the second redox phase, except that the characteristic peak intensity of LSCFRu and ex-solved LSCFRu are disappeared, which is consistent with previous studies [41,42]. The sensors were named LSCF (Parent host), LSCFRu (Ex0, before reduction), (Ex 450 $^\circ\text{C}$, reduction at 450°C). These findings suggest that CoFeRu was fully dissolved in the LSCF lattice with a negative shift in XRD peaks suggesting a change in lattice parameter (Figure S2). The increased lattice parameter signals the substitution of bigger Ru^{4+} with smaller Fe^{3+} ions [43]. A minor amount of CoFe_2O_4 is also formed due to the A-site deficiency. After the reduction in H_2 atmosphere, the CoFe phase (PDF#49-1568; Pm-3 m) emerged. The SEM images revealed the generation of CoFe NPs which increases with Ru-doped LSCF electrodes showing enhanced ex-solution in the presence of Ru-dopants. The TEM images of LSCFRu at 450°C is shown in Fig. 2i-j. The surface morphology of Ex_450 is shown in Figure S3. The observations revealed that the LSCFRu underwent ex-solution of CoFeRu NPs on their surfaces at temperatures $< 400^\circ\text{C}$, which is the lowest temperature reported for ex-solution of NPs (Tables S1). The ex-solved NPs were less than 10 nm and observed on the surfaces of the LSCFRu during the in-situ reduction processes. A single ex-solved NP was imaged using HR-TEM and FFT pattern as shown in Fig. 2i-j. The interplanar spacing corresponding to the (121) plane was 0.28 nm. Direct measurements of the NPs in various areas showed that their size, density, and total volume increased with

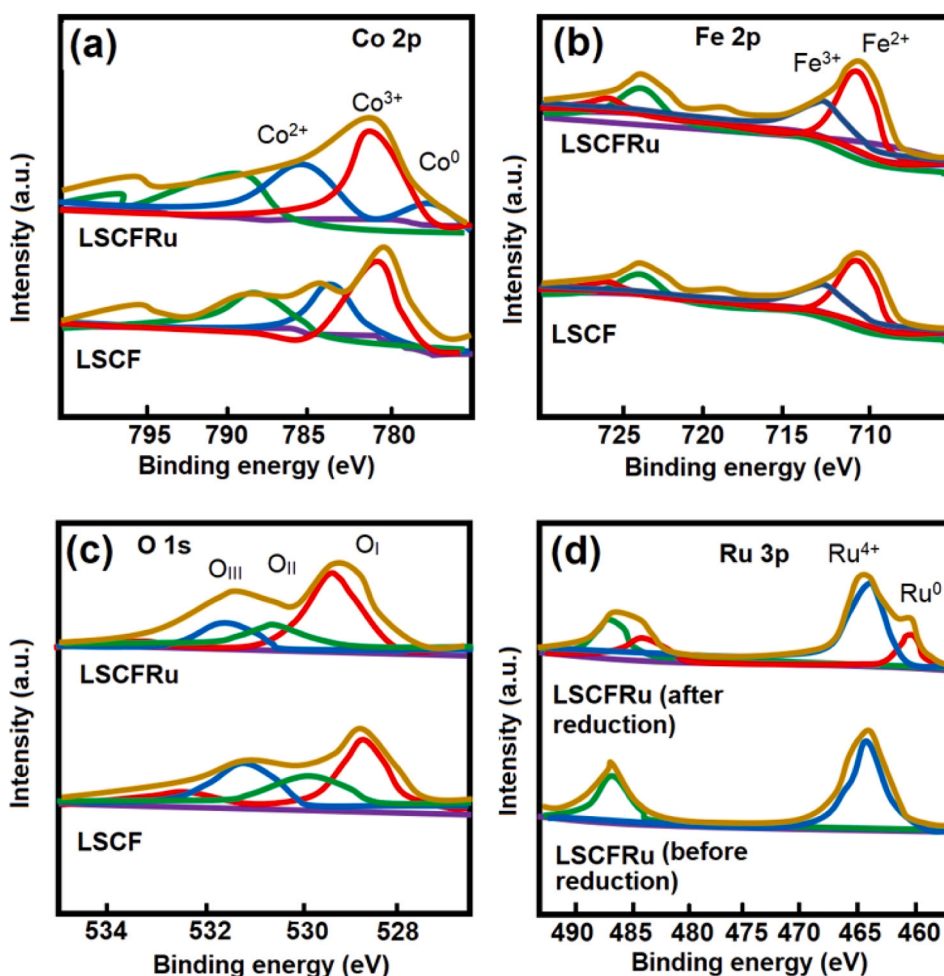


Fig. 3. The de-convoluted spectra of (a) Co2p, (b) Fe2p, (c) O 1 s, (d) and Ru3p in LSCF and LSCFRu (Ex_450).

temperature, which can be explained by the increase in ex-solving tendency as the reduction temperature rises (as shown in Fig. 2i,j, and Table S1). This type of low-temperature ex-solution process prevented further sintering of the host structure, even after annealing at 550 °C. The specific surface area of the resulting CoFeRu-ex-solved LSCFRu electrodes remained similar to that of LSCF, indicating that this approach is effective in broadening the scope of other catalytic materials.

The chemical survey and high-resolution XPS analysis of Ex0, Ex_350, Ex_450, and Ex_550 sensors are presented in Fig. 3. The presence of La, Sr, Co, Fe, and Ru was confirmed. The C 1 s peak was used as the calibration point for the measured spectra, which were found to have Co³⁺ and Co²⁺ peaks at around ~779.3 and ~795.1 eV, and ~781.2 and ~796.3 eV, respectively, for the different samples (Fig. 3a). The amount of [Co³⁺]/[Co²⁺], and various chemisorbed oxygens are shown in Table S2. The [Co³⁺]/[Co²⁺] ratios for LSCF and LSCFRu (Ex_450) are 2.03 and 1.44, respectively. This ratio decreased after the ex-solution process, indicating the detachment of oxygen from cobalt oxide (Co³⁺) and an increase in metallic cobalt (Co²⁺) uniformly distributed on the LSCFRu surface [44]. There was no Fe2p peak due to a higher concentration of Fe in undoped LSCF. In LSCFRu, Fe²⁺ and Fe³⁺ were located at about 711 and 713 eV (Fig. 3b) [45]. The fraction [Fe³⁺]/[Fe²⁺] was also decreased in LSCFRu indicating a lower proportion of Fe³⁺ leading to the alloying of Fe in ex-solved NPs after reduction (Table S2).

The O 1 s peaks of all samples enclose different kinds of oxygen peaks: lattice oxygen (O_I: 529.4 eV), oxygen-devoid peak (O_{II}: 530.5 eV), and chemisorbed oxygen (O_{III}: 531.9 eV). The O_I intensity was higher than that of O_{II}, but O_I decreased gradually and O_{II} increased as the reduction temperature increased (Fig. 3c). The binding energy of O_{II} shifts to positive with Ru doping indicating strong metal-oxygen bonding in LSCFRu [46]. After reduction, the binding energy of O_{II} moves to the negative side showing the change in oxygen vacancies after reduction [47,48]. Ex_450 generated the most oxygen vacancy due to lattice oxygen migration reacting with hydrogen, leading to lattice expansion, resulting in the highest value of O_{II}. Oxygen-devoid and chemisorbed oxygen (O_I, O_{III}) enhance the gas adsorption kinetics, and Ex_450 is expected to exhibit higher gas response due to the highest value of [O_{II}+O_{III}] and the decreased [Co³⁺]/[Co²⁺] ratio among the samples. Notably, Ru⁴⁺ (463.8 eV) and Ru⁰ (461.1 eV) are found in Ru3p of LSCFRu after reduction while Ru⁴⁺ exists only in LSCFRu

(Fig. 3d).

Finally, we demonstrate the potential of CoFeRu-exsolved LSCF layers toward hydrogen gas sensing. Ex-solution processes have typically been employed in high-temperature catalyst supports and fuel cells. A few notable attempts have been made to create PdO-ex-solved LaFePd_{0.05}O_{3+x} host oxide for impedance metric gas sensor applications [19,20]. Recent investigations by Kim et al., have shown promising ethanol gas sensing of Co-ex-solved La_{0.43}Ca_{0.37}Co_{0.06}Ti_{0.94}O_{3-d} [36]. Unfortunately, these attempts have been hindered by unwanted particle growth owing to a high reduction temperature used for ex-solution and calcination temperatures. In our investigations, we developed a low-temperature ex-solution technique for multi-metallic CoFeRu NPs on the LSCFRu system. We have compared our results with the previous low temperature ex-solution process in oxide and other precious metals (Table 1). Our work demonstrates a comparable operating temperature for the ex-solved perovskite sensors.

The use of a low-temperature ex-solution process enabled us to maintain the high porosity of host oxide having a high specific surface area resulting in a significant rise in the gas response.

In Fig. 4a, we compared the H₂ sensing characteristics of the as-prepared different sensors towards H₂, NO, HCHO, NH₃, NO₂, and CO measured at 350–550 °C. The sensing properties were not measured at temperatures below 350 °C because the high resistance in air made it difficult to achieve a prompt recovery and reaction time. When n-type LSCFRu is exposed to air, oxygen molecules are adsorbed on the surface. Due to the electrons transfer from the oxide to the surface, the development of potential barriers on the particle surface occurs, which affects relatively few oxygen adsorption sites available on the n-type semiconductor surface. For conductance, electrons must pass over this surface barrier to move from one particle to the next. Depending on the temperature, adsorbed oxygen ion species (O²⁻, O⁻, and O₂⁻) are formed by the extraction of conduction band electrons and by generating a space charge conduction area. This causes an increase in sensor resistance [9, 60].

Although most samples exhibited an increase in gas response as the operating temperature increased, they eventually reached a maximum gas response and then experienced a decrease in gas response with further temperature increases. The Ex_450 sensor response to 0.1–5 ppm H₂ was measured at 450 °C, and the LOD was estimated to be 0.05 ppm by extrapolating the response data in Fig. 4a as the sensing

Table 1

Previous ex-solution processes in oxide and precious metals.

Ex-solved hydrogen gas sensors					
Ex-solved particles/host oxides	Ex-solution temperature	Ex-solution time	Gas atmosphere	Application	Ref.
CoFeRu(La _{0.8} Sr _{0.2}) _{0.9} Co _{0.1} Fe _{0.8} Ru _{0.1} O _{3-δ}	350 °C	4 h	15 % H ₂	Hydrogen sensing	Present study
Ni/La _{0.4} Sr _{0.4} Sc _{0.9} Ni _{0.1} O ₃	900 °C	15 h	Pure H ₂	SOFC	[49]
Co/Pr _{0.5} Ba _{0.5} MnO ₃	850 °C	4 h	10 % H ₂ /N ₂	Electrochemical	[50]
Ru/(La _{0.8} Sr _{0.2}) _{0.9} Sc _{0.2} Mn _{0.8} O _{3-d}	900 °C	20 h	5 % H ₂ /N ₂	SOFC	[51]
Fe/La _{0.4} Sr _{0.4} Fe _x Ti _{1-x} O _{3-d}	930 °C	20 h	5 % H ₂ /N ₂	N/A	[52]
Ni-Co/LaNi _{0.9} Co _{0.1} O ₃	700 °C	2 h	Pure H ₂	SOFC	[53]
Pd/LaFePd _{0.05} O _{3+d}	700 °C	0.5 h	10 % H ₂ /air	Gas sensor	[54]
Ni/La _{0.43} Ca _{0.37} Ni _{0.06} Ti _{0.94} O _{3-d}	900 °C	<150 ms	50 % H ₂ O/ N ₂	SOFC	[55]
Ir/WO ₃ NFs	400 °C	1 h	4 % H ₂ /air	Gas sensor	[56]
Rh/IPL1_Rh-WO ₃ NFs	>900 °C	<20 ms	Ambient conditions	Gas sensor	[57]
Ag/AgNbO ₃	300 °C	1 h	10 % H ₂ /Ar	Gas sensor	[58]
Pd/LaFe _{0.95} Pd _{0.05} O ₃	300 °C	3 h	10 % H ₂ /He	CH ₄ combustion	[59]
RT Hydrogen gas sensors					
MoSi ₂ -SnO ₂	10 ppm	120 °C	12 s	27 s	[60]
Pd/porous Si Schottky	100–40,000 ppm	RT	7 s	1500 s	[61]
Pt/In ₂ O ₃	0.5–3 %	RT	33 s	66 s	[62]
α-MoO ₃	500 ppb–1000 ppm	RT	14 s	75 s	[63]
Chalcogenides (Bi ₂ Te ₃ , Sb ₂ Te ₃)	40 ppm–45 vol%	RT	1.3	NA	[64]
Pd/MWCNT/Graphene	10–10,000 ppm	RT	600 s	300 s	[65]
Pt/SnO ₂ nanorods	1000 ppm	RT	0.33 s	29.6 s	[66]
Reduced graphene oxide/SnO ₂ / polyvinylidene fluoride nanocomposite	100 ppm	RT	34 s	142 s	[67]
Polyaniline/SnO ₂ /Pd	50 ppm	RT	39	53	[68]

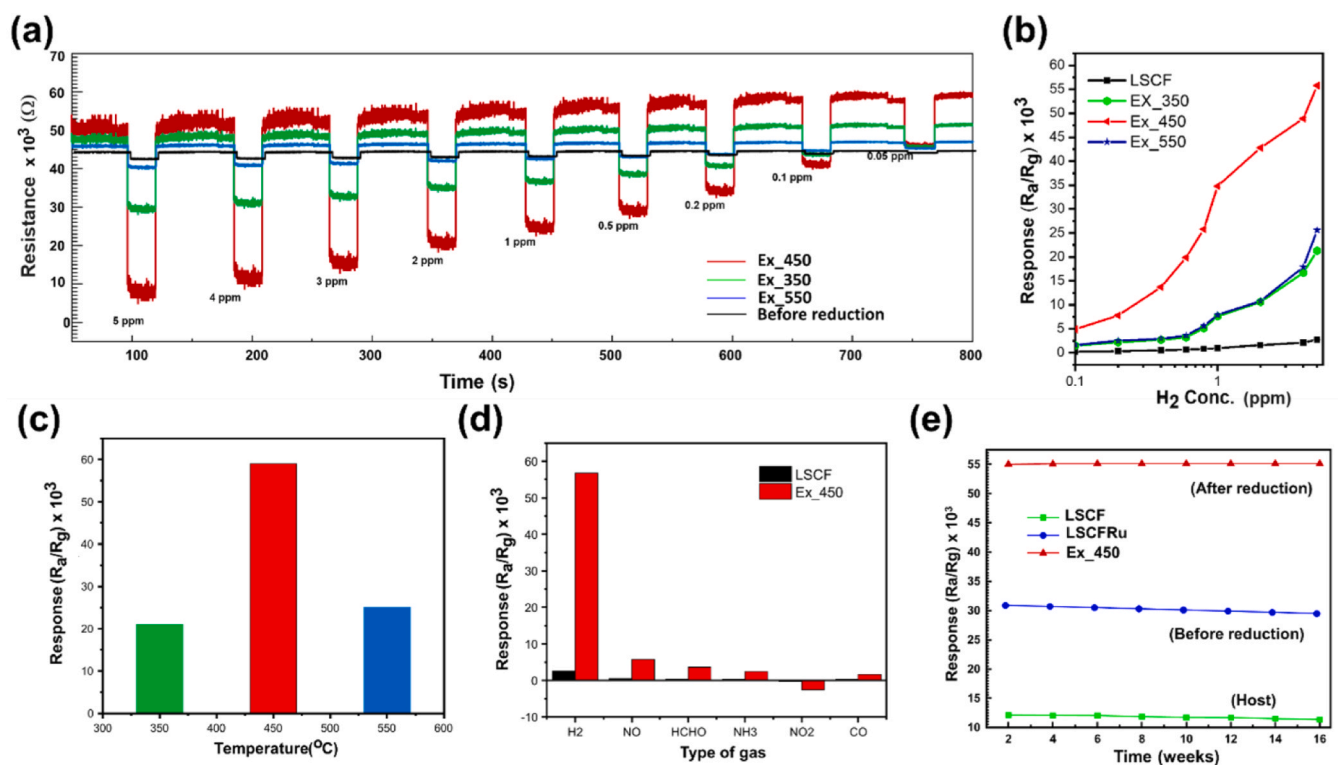


Fig. 4. (a) Dynamic resistance response transitions (in air and H₂) of LSCFRu (before reduction), Ex₃₅₀, Ex₄₅₀, and Ex₅₅₀ at 5 ppm H₂. (b) Gas response of LSCF, ex-solved LSCFRu at 350, 450, and 550 °C at 5 ppm, (c) Temperature-dependent H₂ gas response of ex-solved LSCFRu at 350, 450, and 550 °C at b: 0.1–5 ppm and c: 5 ppm. (d) Selective gas-sensing characteristics of LSCF (un-doped) and Ex₄₅₀, (e) Long-term stability of LSCF, LSCFRu before reduction and Ex₄₅₀ at 5 ppm H₂.

criterion for gas detection (Fig. S4). The results confirmed the effectiveness of the CoFeRu NPs by the ex-solution method as the catalytic effect of H₂ gas sensing. The base LSCF (undoped) showed a typical chemiresistive p-type gas response while Ex₃₅₀, Ex₄₅₀, and Ex₅₅₀ exhibited n-type MOX behavior (Fig. 4b). The most probable explanation for the observed p-type to n-type shift in ex-solved LSCFRu seems to be that we are situated in an intermediate region regarding the defect chemistry, transitioning from ionic conduction by oxygen vacancies as minority carriers to electronic conduction by electrons as majority carriers. It is noticed that the Ex₄₅₀ sensor demonstrated a substantial response to H₂ compared to Ex₀ (before reduction, LSCFRu, Fig. 4c). The surface area of Ex₃₅₀ CoFeRu NPs was not enough to observe considerable gas response due to insufficient spill-over of CoFeRu NPs. However, the Ex₅₅₀ was able to observe aggregation of CoFeRu NPs at high temperatures that resulted in lower surface area and growth of NPs [36]. As a consequence, the Ex₅₅₀ sensor was unable to function as a gas sensor due to the occurrence of aggregation of ex-solution particles, which resulted in a low gas response. Thus, the optimal ex-solution temperature for superior H₂ gas sensing was confirmed to be at 450 °C according to the temperature dependent H₂ gas response behavior. This suggests that the ex-solved CoFeRu NPs were primarily responsible for the significant improvement in H₂ gas response characteristics. While LSCF showed poor selectivity for 5 ppm H₂, Ex₄₅₀ showed a dramatically improved H₂ selectivity with negligible gas response to other gas species. The gas response of un-doped LSCF showed a minute variation ($R_a/R_g < 10$ at 5 ppm NO, HCHO, NH₃, NO₂, and CO, Fig. 4d). The sample Ex₄₅₀ exhibited the highest H₂ response ($R_a/R_g = 55$ at 5 ppm H₂, 450 °C), which was over 20 times higher compared to LSCF (un-doped) ($R_a/R_g = 2.5$ at 5 ppm). Furthermore, as discussed earlier, the XPS O1s peak for the Ex₄₅₀ sensor shows a higher ratio of oxygen deficiency compared to Ex₀, which is attributed to the catalytic effect of CoFeRu-ex-solved NPs due to a higher electronic charge distribution [35,36,48,69], CoFeRu –ex-solved NPs can release more electrons than

LSCF, resulting in the adsorption of more oxygen species on LSCF. Previous studies have shown that ex-solved NPs are highly resistant to sintering and coking behavior owing to their socketing structure [30]. Similarly, the optimized gas sensor, Ex₄₅₀ maintained its stable H₂ gas response during long H₂ response cycles for 5 ppm (> 16 weeks), while undoped LSCF and LSCFRu before reduction indicated a decreased H₂ gas response, resulting in poor stability (Fig. 4e). These findings suggest that the Ex₄₅₀ sensor is a promising and reliable candidate for H₂ gas sensing.

The response and recovery values of Ex₀ (LSCFRu, before reduction) were 42 s and 67 s, respectively for 5 ppm H₂. (Fig. S5). In contrast to LSCF and LSCFRu, the Ex₄₅₀ sensor demonstrated a much faster response, with t_{res} and t_{rec} of 15 s and 29 s, respectively. In comparison, undoped LSCF showed an inferior response ($t_{res} = 50$ s) and recovery time ($t_{rec} = 74$). This result indicates that CoFeRu-exsolved NPs facilitate the gas response kinetics through their catalytic activity [33]. Consequently, CoFeRu-exsolved NPs of LSCFRu, with various characteristics such as gas sensing properties, chemical stability, and thermal stability, could be suitable for use in various industrial applications. Specifically, we observed that the presence of multi-metallic CoFeRu dopants facilitated the phase transformation of the host LSCF and enhanced the efficiency of the ex-solution process.

3.1. Gas sensing mechanism

As mentioned previously, the Ex₀ sensor operates as a typical p-type semiconductor, while the Ex₃₅₀, Ex₄₅₀, and Ex₅₅₀ sensors are n-type semiconductors due to the metallic character of CoFeRu NPs. The gas sensing mechanism of the ex-solution-derived sensors is thus proposed to be the synergistic effects of electronic and chemical sensitization as shown in Fig. 5. The electronic sensitization mechanism changes the charge carrier concentration by using the ex-solution method [36]. The uniformly dispersed CoFeRu-exsolved NPs in ex-solved sensors expand

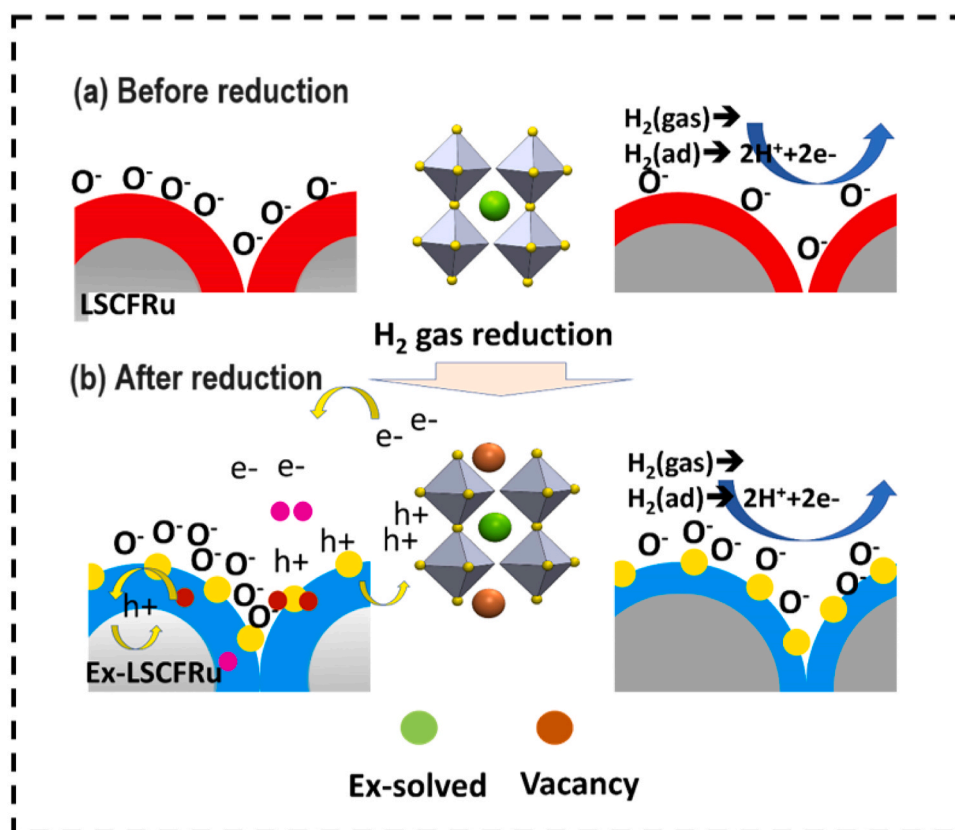


Fig. 5. Mechanism of gas sensing for ex-solved LSCFRu. (a) Before and (b) after reduction.

the electric double layer (EDL) under the CoFeCu NPs, which reduces the conduction path and raises the resistance response in air. As a result, the EDL can penetrate deep into the LSCF, and the gas response rises.

To enhance the gas response, La-Sr-O catalysts have been reported in the literature to provide suitable adsorption-desorption sites via the chemical spillover effect. Moreover, perovskite with extreme oxygen vacancies will promote the mobility of oxygen ions and adsorb oxygen species from the surface of the catalyst by the spillover effect and react with more reduction gas. After gas exposure, the EDL and the hole accumulation layer (HAL) around the CoFeRu NPs become very thin. The significant increase in resistance in air indicates that ex-solved CoFeRu NPs have a strong effect on LSCF [36]. It can be seen that p-type LSCFRu is switched to n-type via the ex-solution of CoFeRu NPs. According to the perovskite oxide (La-Sr-O) and ex-solved particles (CoFeRu) result, the perovskite oxide is n-type perovskite; however, CoFeRu acted as p-type precipitates with cobalt concentration. The observed p-to n-type transition of ex-solved LSCFRu is explained by the defect chemistry of host oxide which evolves from the minor ionic conduction (oxygen vacancies) to the majority of electronic conduction by introduction of ex-solved n-type CoFeRu NPs. The p-n type switching is favorable to achieve the n-type metallic character and move the Fermi level as close to the conduction band after reduction [36]. For most of the p-type perovskites, such as in the present study, Co-, and Fe-dopants in the LSCF are originally p-type. However, during the ex-solution process, CoFeRu NPs were uniformly distributed on the surface of LSCF, resulting in a large surface area and oxygen vacancies, which caused a transition from p- to n-type. After the ex-solution technique, ex-solved (La-Sr-O) exhibits n-type perovskite due to the weaker metal-oxygen (Co-O, Fe-O) bonds, an increase in oxygen vacancy, and a reduction in Co concentration of the parent structure. The CoFeRu NPs grown from the LSCF surface are oxidized to p-type La-Sr-O, and CoFeRu NPs exhibit n-type characteristics. As a result, the EDL is widened by electronic sensitization at the point of contact, and ex-solution LSCF has higher

resistance due to the uniformly distributed CoFeRu-ex-solved NPs on the ex-solved LSCF layer via p-n transition. Upon exposure to H₂ gas, the wider EDL under the CoFeRu-ex-solved NPs rapidly changes into a thin layer, leading to a significant enhancement in gas response.

4. Conclusions

In this study, we designed a rational approach to create uniformly distributed solid solution NPs, specifically, CoFeRu, on a perovskite host Ru-doped LSCF for hydrogen gas sensing. This was achieved through a low-temperature ex-solution process (approximately 350°C). The ex-solution process was influenced by the temperature, which affected the size and quantity of CoFeRu-ex-solved NPs on the perovskite surface. The gas sensing characteristics of the perovskite host were significantly enhanced, with the sensing response almost approached 20 times after reduction at 450 °C with LOD of 0.05 ppm. The gas sensing mechanism of the ex-solved LSCFRu sensors was thus proposed to be the synergistic effects of electronic and chemical sensitization. The strong attachment and fine distribution of CoFeRu NPs to the host oxide resulted in improved gas response and recovery with high selectivity towards a mixture of H₂, NO, NO₂, HCHO, NH₃ and CO gases. The enhanced H₂ gas response is ascribed to the catalytic activity of the ex-solved CoFeRu NPs on the perovskite host at a low temperature, as well as the p-to-n-type transition after reduction. The ex-solved perovskite demonstrated excellent chemical, thermal, and long-term gas response stability. Overall, this study introduces a new research path that expands the current paradigm of ex-solution-derived chemiresistors.

CRediT authorship contribution statement

Bharat Sharma: Writing – review & editing, Writing – original draft, Supervision, Methodology, Investigation, Funding acquisition, Data curation, Conceptualization. **Mukesh Kumar:** Visualization, Software,

Formal analysis, Data curation. **Ashutosh Sharma:** Writing – review & editing, Writing – original draft, Methodology, Formal analysis, Data curation.

Declaration of Competing Interest

The authors declare that they have no known competing financial interests or personal relationships that could have appeared to influence the work reported in this paper.

Data Availability

Data will be made available on request.

Acknowledgements

This work was partly supported by the Deutsche Forschungsgemeinschaft (DFG, German Research Foundation) under Germany's Excellence Strategy via the Excellence Cluster 3D Matter Made to Order (EXC-2082/1-390761711).

Conflict of interest statement

The authors declare no conflict of interest.

Appendix A. Supporting information

Supplementary data associated with this article can be found in the online version at [doi:10.1016/j.snb.2024.136529](https://doi.org/10.1016/j.snb.2024.136529).

References

- Isolde Simon, Nicolae Baarsan, Michael Bauer, Udo Weimar, Micro-machined metal oxide gas sensors: opportunities to improve sensor performance, *J. Sens. Actuators Vol. 73* (No. 18) (2001) 11–26.
- M. Aslam, C. Gregory, J.V. Hatfield, Polyimide membrane for micro-heated gas sensor array, *Sens. Actuator B* 103 (2004) 153–157.
- W.J. Buttner, M.B. Post, R. Burgess, C. Rivkin, An overview of hydrogen safety sensors and requirements, *Int. J. Hydrog. Energy* 36 (2011) 2462–2470.
- C. Wadell, S. Syrenova, C. Langhammer, Plasmonic hydrogen sensing with nanostructured metal hydrides, *ACS Nano* 8 (2014) 11925–11940.
- P.S. Chauhan, S. Bhattacharya, Hydrogen gas sensing methods, materials, and approach to achieve parts per billion level detection: a review, *Int. J. Hydrog. Energy* 44 (2019) 26076–26099.
- F.A. Nugroho, et al., Metal–polymer hybrid nanomaterials for plasmonic ultrafast hydrogen detection, *Nat. Mater.* 18 (2019) 489.
- G. Korotcenkov, Metal oxides for solid-state gas sensors: what determines our choice? *Mater. Sci. Eng.: B* 139 (2007) 1–23.
- L. Zhang, K. Khan, J.F. Zou, H. Zhang, Y.C. Li, Recent advances in emerging 2D material-based gas sensors: potential in disease diagnosis, *Adv. Mater. Interfaces* 6 (2019) 1901329.
- B. Sharma, A. Sharma, J.S. Kim, Recent advances on H₂ sensor technologies based on MOX and FET devices: a review, *Sens. Actuators B* 262 (2018) 758–770.
- R. You, X. Hao, H. Yu, B. Wang, G. Lu, et al., High performance mixed-potentialtype Zirconia-based NO₂ sensor with self-organizing surface structures fabricated by low energy ion beam etching, *Sens. Actuators B Chem.* 263 (2018) 445–451.
- G. Korotcenkov, S.D. Han, J.R. Stetter, Review of electrochemical hydrogen sensors, *Chem. Rev.* 109 (2009) 1402–1433.
- J.R. Stetter, J. Li, Amperometric gas sensors—a review, *Chem. Rev.* 108 (2008) 352–366.
- E.D. Bartolomeo, M.L. Grilli, J.W. Yoon, E. Traversa, Zirconia-based electrochemical NO_x sensors with semiconducting oxide electrodes, *J. Am. Ceram. Soc.* 87 (2004) 1883–1889.
- H. Zhang, J. Yi, X. Jiang, Fast response, highly sensitive and selective mixed-potential H₂ sensor based on (La, Sr)(Cr, Fe)O₃-delta perovskite sensing electrode, *ACS Appl. Mater. Interfaces* 9 (2017) 17218–17225.
- W. Xiong, G.M. Kale, Electrochemical NO₂ sensor using a NiFe_{1.9}Al_{0.1}O₄ oxide spinel electrode, *Anal. Chem.* 79 (2007) 3561–3567.
- S. Kim, et al., Nanostructured double perovskite cathode with low sintering temperature for intermediate temperature solid oxide fuel cells, *ChemSusChem* 8 (2015) 3153–3158.
- R.J. Gorte, J.M. Vohs, Nanostructured anodes for solid oxide fuel cells, *Curr. Opin. Colloid Interface Sci.* 14 (2009) 236–244.
- M.V.F. Schlupp, A. Evans, J. Martynczuk, M. Prestat, Micro-solid oxide fuel cell membranes prepared by aerosol-assisted chemical vapor deposition, *Adv. Energy Mater.* 4 (2014) 1301383.
- D. Neagu, G. Tsekouras, D.N. Miller, H. Ménard, J.T. Irvine, *Nat. Chem.* 5 (2013) 916.
- Xu Li, Lei Dai, Zhangxing He, Wei Meng, Yuehua Li, Ling Wang, In situ exsolution of PdO nanoparticles from non-stoichiometric LaFePd_{0.05}O_{3+δ} electrode for impedancemetric NO₂ sensor, *Sens. Actuators: B. Chem.* 298 (2019) 126827.
- Xu Li, Lei Dai, Zhangxing He, Wei Meng, Yuehua Li, Ling Wang, Enhancing NH₃ sensing performance of mixed potential type sensors by chemical exsolution of Ag nanoparticle on AgNbO₃ sensing electrode, *Sens. Actuators B: Chem.* 298 (2019) 126854.
- J.H. Kim, J.K. Kim, H.G. Seo, D.K. Lim, S.J. Jeong, J. Seo, J. Kim, W. Jung, *Adv. Funct. Mater.* 30 (2020) 2001326.
- K.-Y. Lai, A. Manthiram, Self-regenerating Co–Fe nanoparticles on perovskite oxides as a hydrocarbon fuel oxidation catalyst in solid oxide fuel cells, *Chem. Mater.* 30 (2018) 2515–2525.
- W. Zhou, Z. Shao, F. Liang, Z.-G. Chen, Z. Zhu, et al., A new cathode for solid oxide fuel cells capable of in situ electrochemical regeneration, *J. Mater. Chem.* 21 (2011) 15343–15351.
- J. Tan, D. Lee, J. Ahn, B. Kim, J. Kim, et al., Thermally driven in situ exsolution of Ni nanoparticles from (Ni, Gd)CeO₂ for high-performance solid oxide fuel cells, *J. Mater. Chem. A Mater. Energy Sustain.* 6 (2018) 18133–18142.
- Y.-F. Sun, J.-H. Li, M.-N. Wang, B. Hua, J. Li, et al., A-site deficient chromite perovskite with in situ exsolution of nano-Fe: a promising bi-functional catalyst bridging the growth of CNTs and SOFCs, *J. Mater. Chem. A Mater. Energy Sustain.* 3 (2015) 14625–14630.
- L. Dai, L. Ma, W. Meng, Y. Li, Z. He, et al., Impedancemetric NO₂ sensor based on Pd doped perovskite oxide sensing electrode conjunction with phase angle response, *Electrochim. Acta* 265 (2018) 411–418.
- H.T. Giang, H.T. Duy, P.Q. Ngan, G.H. Thai, D.T.A. Thu, et al., High sensitivity and selectivity of mixed potential sensor based on Pt/YSZ/SmFeO₃ to NO₂ gas, *Sens. Actuators B Chem.* 183 (2013) 550–555.
- L. Wang, Y. Wang, L. Dai, Y. Li, J. Zhu, et al., High temperature amperometric NO₂ sensor based on nano-structured Gd_{0.2}Sr_{0.8}FeO_{3–δ} prepared by impregnating method, *J. Alloy. Compd.* 583 (2014) 361–365.
- D. Neagu, et al., Nano-socketed nickel particles with enhanced coking resistance grown in situ by redox exsolution, *Nat. Commun.* 6 (2015) 8120.
- Xing-Hua Ma, Hua-Yao Li, Sang-Hyo Kweon, Seong-Yong Jeong, Jong-Heun Lee, Sahn Nahm, Highly sensitive and selective PbTiO₃ gas sensors with negligible humidity interference in ambient atmosphere, *ACS Appl. Mater. Interfaces* 11 (5) (2019 Feb 6) 5240–5246.
- Changmin Shi, Hongwei Qin, Ming Zhao, Xiaofeng Wang, Ling Li, Jifan Hu, Investigation on electrical transport, CO sensing characteristics and mechanism for nanocrystalline La_{1–x}CaxFeO₃ sensors, *Sens. Actuators B: Chem.* 190 (2014) 25–31.
- Ji-Soo Jang, Jun Kyu Kim, Kyeounghak Kim, Wan-Gil Jung, Chaesung Lim, Sangwoo Kim, Dong-Ha Kim, Bong-Joong Kim, Jeong Woo Han, WooChul Jung, Il-Doo Kim, Dopant-driven positive reinforcement in ex-solution process: new strategy to develop highly capable and durable catalytic materials, *Adv. Mater.* (2020) 2003983.
- Pengfei Cao, Pengyi Tang, Maged F. Bekheet, Hongchu Du, Luyan Yang, Leander Haug, Albert Gili, Benjamin Bischoff, Aleksander Gurlo, Martin Kunz, Rafal E. Dunin-Borkowski, Simon Penner, Marc Heggen, Atomic-scale insights into nickel exsolution on LaNiO₃ catalysts via in situ electron microscopy, *J. Phys. Chem. C* 126 (2022) 786–796.
- Ohhun Kwon, Sivaprakash Sengodan, Kyeounghak Kim, Gihyeon Kim, Hu. Young Jeong, Jeeyoung Shin, Young-Wan Ju, Jeong Woo Han, Guntae Kim, Exsolution trends and co-segregation aspects of self-grown catalyst nanoparticles in perovskites, *Nat. Comm.* 8 (2017) 15967.
- Hyeongwon Jeong, Bharat Sharma, Jae-ha Myung, In situ exsolution catalyst: an innovative approach to develop highly selective and sensitive gas sensors, *ACS Appl. Mater. Interfaces* 14 (16) (2022) 18275–18282.
- X. Duan, G. Qian, X. Zhou, D. Chen, W. Yuan, *Chem. Eng. J.* 207–208 (2012) 103–108.
- C. Chen, Y. Chen, A.M. Ali, W. Luo, J. Wen, L. Zhang, H. Zhang, *Chem. Eng. Technol.* 43 (2020) 719–730.
- I. Lucentini, G.G. Colli, C.D. Luzi, I. Serrano, O.M. Martínez, J. Llorca, *Appl. Catal. B* 286 (2021) 119896.
- V.M. Goldschmidt, *Naturwissenschaften* 14 (1926) 477–485.
- Yi Liang, Yu Cui, Yang Chao, Ning Han, Jaka Sunarso, Ping Liang, Xin He, Chi Zhang, Shaomin Liu, Ex-solution of CoFe(Ru) Nanoparticles in Ru-doped (La_{0.8}Sr_{0.2})_{0.9}Co_{0.1}Fe_{0.8}Ru_{0.1}O_{3–δ} for efficient oxygen evolution reaction, *Nano Res.* 15 (8) (2022) 6977–6986.
- H. Lv, L. Lin, X. Zhang, R. Li, Y. Song, H. Matsumoto, N. Ta, C. Zeng, Q. Fu, G. Wang, X. Bao, Promoting exsolution of RuFe alloy nanoparticles on Sr₂Fe_{1.4}Ru_{0.1}Mo_{0.5}O_{6–δ} via repeated redox manipulations for CO₂ electrolysis, *Nat. Comm.* 12 (2021) 5665.
- M. Qin, Y. Xiao, H. Yang, T. Tan, Z. Wang, X. Fan, C. Yang, *Appl. Catal. B* 299 (2021) 120613.
- Yi-Fei Sun, Ya-Qian Zhang, Jian Chen, Jian-Hui Li, Ying-Tao Zhu, Yi-Min Zeng, Babak Shalchi Amirkhiz, Jian Li, Bin Hua, Jing-Li Luo, New opportunity for in situ exsolution of metallic nanoparticles on perovskite parent, *Nano Lett.* 16 (8) (2016) 5303–5309.
- Zhishan Li, Lin Lv, Jinsong Wang, Xiang A, Yunjun Ruan, Dace Zha, Guo Hong, Qihui Wu, Yucheng Lan, Chundong Wang, Jianjun Jiang, Meilin Liu, *Engineering*

- phosphorus-doped LaFeO_{3-δ} perovskite oxide as robust bifunctional oxygen electrocatalysts in alkaline solutions, *Nano Energy* 47 (2018) 199–209.
- [46] Yangli Pan, Xiaomin Xu, Yijun Zhong, Lei Ge, Yubo Chen, Jean-Pierre Marcel Veder, Daqin Guan, Ryan O'Hayre, Mengran Li, Guoxiong Wang, Hao Wang, Wei Zhou, Zongping Shao, Direct evidence of boosted oxygen evolution over perovskite by enhanced lattice oxygen participation, *Nat. Comm.* 11 (2020) 2002.
- [47] Sivaprakash Sengodan Ohhun Kwon, Gihyeon Kim Kyeounghak Kim, Jeeyoung Shin Hu Young Jeong, Jeong Woo Han Young-Wan Ju, Guntae Kim, Exsolution trends and co-segregation aspects of self-grown catalyst nanoparticles in perovskites, *Nat. Comm.* 8 (2017) 15967.
- [48] Ohhun Kwon, Sangwook Joo, Sihyuk Choi, Sivaprakash Sengodan, Guntae Kim, Review on exsolution and its driving forces in perovskites, *J. Phys. Energy* 2 (2020) 032001.
- [49] Y. Gao, D. Chen, M. Saccoccio, Z. Lu, F. Ciucci, *Nano Energy* 27 (2016) 499.
- [50] Y.-F. Sun, J.-H. Li, Y.-Q. Zhang, B. Hua, J.-L. Luo, *ACS Catal.* 6 (2016) 2710.
- [51] J. Zhou, N. Wang, J. Cui, J. Wang, J. Yang, Z. Zong, Z. Zhang, Q. Chen, X. Zheng, K. Wu, *J. Alloy. Compd.* 792 (2019) 1132.
- [52] D. Neagu, G. Tsekouras, D.N. Miller, H. Ménard, J.T. Irvine, *Nat. Chem.* 5 (2013) 916.
- [53] T. Gan, G. Ding, X. Zhi, L. Fan, N. Hou, X. Yao, P. Li, Y. Zhao, Y. Li, *Catal. Today* 327 (2019) 220.
- [54] Y.-F. Sun, Y.-Q. Zhang, J. Chen, J.-H. Li, Y.-T. Zhu, Y.-M. Zeng, B.S. Amirkhiz, J. Li, B. Hua, J.-L. Luo, *Nano Lett.* 16 (2016) 5303.
- [55] H.G. Jeong, D. Kim, B. Sharma, J.H. Noh, K.T. Lee, J.-H. Myung, *Korean J. Chem. Eng.* volume 37 (2020) 1440–1444.
- [56] J.S. Jang, J.K. Kim, K. Kim, W.G. Jung, C. Lim, S. Kim, D.H. Kim, B.J. Kim, J. W. Han, W. Jung, I.D. Kim, Dopant-Driven Positive Reinforcement in Ex-Solution Process: New Strategy to Develop Highly Capable and Durable Catalytic Materials, *Adv. Mater.* 32 (46) (2020) 2003983.
- [57] Y. Jiang, Z. Geng, L. Yuan, Y. Sun, Y. Cong, K. Huang, L. Wang, W. Zhang, *ACS Sustain. Chem. Eng.* 6 (2018) 11999.
- [58] X. Li, L. Dai, Z. He, W. Meng, Y. Li, L. Wang, *Sens. Actuators B: Chem.* 298 (2019) 126854.
- [59] A. Eyssler, P. Mandaliev, A. Winkler, P. Hug, O. Safonova, R. Figi, A. Weidenkaff, D. Ferri, *J. Phys. Chem. C.* 114 (2010) 4584.
- [60] A. Sharma, B. Sharma, Influence of microheater patterns: MoSi₂-SnO₂ as energy-saving chemiresistors for gas sensing applications, *Sens. Actuators B: Chem.* 351 (2022) 130901.
- [61] F. Razi, A. Iraj, F. Rahimi, Investigation of hydrogen sensing properties and aging effects of Schottky like Pd/porous Si, *Sens Actuators B Chem.* 146 (2010) 53–60.
- [62] Y. Wang, B. Liu, D. Cai, H. Li, Y. Liu, D. Wang, et al., Roomtemperature hydrogen sensor based on grain-boundary controlled Pt decorated In₂O₃ nanocubes, *Sens Actuators B Chem.* 201 (2014) 351–359.
- [63] S. Yang, Z. Wang, Y. Hu, X. Luo, J. Lei, D. Zhou, et al., Highly responsive room-temperature hydrogen sensing of a-MoO₃ nanoribbon membranes, *ACS Appl. Mater. Interfaces* 7 (2015) 9247–9253.
- [64] S. Kim, Y. Lee, Y. Choi, H. Lim, J. Lim, N.V. Myung, et al., Thermochemical hydrogen sensor based on chalcogenide nanowire arrays, *Nanotechnology* 26 (2015).
- [65] U. Yaqoob, A.S.M.I. Uddin, G. Chung, Foldable hydrogen sensor using Pd nanocubes dispersed into multiwall carbon nanotubes-reduced graphene oxide network assembled on nylon filter membrane, *Sens Actuators B Chem.* 229 (2016) 355–361.
- [66] Zihui Chen, Keyang Hu, Piaoyun Yang, Xingxing Fu, Zhao Wang, Shulin Yang, Juan Xiong, Xianghui Zhang, Yongming Hu, Haoshuang Gu, Hydrogen sensors based on Pt-decorated SnO₂ nanorods with fast and sensitive room-temperature sensing performance, *J. Alloy. Compd.* 811 (2019) 152086.
- [67] Deepak Punetha, Manoranjan Kar, Saurabh Kumar Pandey, A new type low-cost, flexible and wearable tertiary nanocomposite sensor for room temperature hydrogen gas sensing, *Sci. Rep.* 10 (2020) 2151.
- [68] Rohit Kumar Pippara, Pankaj Singh Chauhan, Anshul Yadav, Vinay Kishnani, Ankur Gupta, Room temperature hydrogen sensing with polyaniline/SnO₂/Pd nanocomposites, *MNE* 12 (2021) 100086.
- [69] N.W. Kwak, S.J. Jeong, H.G. Seo, S. Lee, Y. Kim, J.K. Kim, P. Byeon, S.-Y. Chung, W. Jung, *Nat. Commun.* 9 (2018) 4829.

Ashutosh Sharma is Associate Professor in the Department of Physics, Amity Institute of Applied Sciences, Amity University Jharkhand, India. Previously, he worked as Assistant Professor in the Department of Materials Science and Engineering, Ajou University, South Korea. He has almost 11 years of research and teaching experience with more than 200 publications and 17 international patents so far. He earned his Doctorate from the Indian Institute of Technology (IIT) Kharagpur, India. His current research interests include gas sensors, additive manufacturing, electrodeposition of metals and corrosion.

Bharat Sharma is a scientist at the Karlsruhe Institute of Technology, Germany, and a member of the Institute of Microstructure Technology. He attained his Ph.D. degree from the University of Seoul, South Korea in field of material science and engineering on title entitled 'Enhancement of the sensing performance of MEMS/MOSFET-type hydrogen sensors using Pd-based alloys and hybrid materials'. He has been Post-doc in materials science and engineering at Incheon National University (Seoul, Republic of Korea). In IMT, he works on project funded entitled 'Integrated Multiscale Nanomanufacturing' by Cluster of Excellence 3D Matter Made to Order (3DMM2O).

Research interest

- 3D printing, additive manufacturing
- Electrospinning
- gas sensors
- Nanofabrication
- Micro-Electro-Mechanical Systems (MEMS)
- Sputtering
- Chemical vapor deposition (CVD)
- Thin-film solid oxide fuel cells (SOFCs)
- In-situ metal/alloy exsolution
- Surface modification by metal nanoparticles